PII: S0955-2219(98)00083-1
Printed in Great Britain. All rights reserved
0955-2219/98/$—see front matter

Study of the Mechanical Properties of Ceramic Materials by the Nanoindentation Technique

J. Woirgard,* C. Tromas, J. C. Girard and V. Audurier

Université de Poiters, Laboratoire de Métallurgie Physique, UMR CNRS 6630, Bd. 3 Téléport 2, B.P. 179, 86960 Futuroscope Cedex, France

(Received 12 November 1997; revised version received 18 February 1998; accepted 25 February 1998)

Abstract

A nanoindentation device has been developed allowing the application of forces ranging between a few micronewtons and 100 milinewtons with nanoindentation capabilities. The apparatus offers also very accurate positioning in three directions through the use of a high resolution tridirectional piezoelectric actuator. One of the main interests of the device is to allow fast and precise measurements in normal laboratory environment, making nanoindentation testing as simple to use as conventional hardness ones. After a short presentation of the device and its working principle and of some of the methods used to derive the mechanical properties of materials, some results concerning the nanoscale plasticity in some ceramic materials are presented. Special features as unloading pop-out in silicon, associated to a reversible densification process, and pop-in or yield points during loading, in GaAs and MgO, are pointed out.
© 1998 Elsevier Science Limited. All rights reserved

1 Introduction

The mechanical properties of ceramic and glass materials have been intensively studied and especially the hardness, which is one of the few means by which the low temperature plasticity of brittle materials can be estimated. Hardness, in conjunction with elastic modulus and fracture toughness, is frequently used to estimate the resistance to abrasion and erosion.

Various indentation techniques are available for hardness measurements of bulk materials and films. In the case of thin films and since the indentation depth must be at least five times smaller than the film thickness, depth sensing indentation methods have been developed, achieving minimum residual depths as low as a few nanometers.[1–3] Such tests involve very small applied load and require extremely precise measurements. The shallow residual plastic impressions involved in these experiments can hardly be evaluated, as in conventional hardness tests, by direct examination. Furthermore, in the case of ceramic materials, the surface of the remaining indents after load removal, is often much smaller than the true contact area under load, between the tip and the sample, since this area continuously changes during unloading.

In this paper, after a presentation of the nanoindentation apparatus, and the methods used to derive the hardness and elastic modulus from experimental curves, some results concerning the nanoscale plasticity of ceramics materials and its special features, will be presented. Dislocation activity, associated with the nanoindentation process, will be also studied in the case of MgO single crystal.

2 Description of the nanoindentation apparatus

Due to large environmental effects, nanoindentation tests, at a very low scale, are difficult and time consuming. The principal reason is the necessity to wait after mounting a specimen, a total thermal stabilization of the machine and its environment. Complex loading sequences are then required attempting to evaluate erratic thermal drifts. As it will be shown later the machine compliance is also an obstacle for rapid hardness and elastic modulus measurements, especially when the mechanical properties of the material vary with the indentation penetration.

It is the reason why the apparatus used in this work, with negligible thermal drifts and compliance, has been developed. Very low thermal drifts have been achieved by making the measurement

*To whom correspondence should be addressed.
E-mail: jacques.woirgard@lmp.univ-poitiers.fr

head in a very low thermal expansion material (fused silica) and applying the force electrostatically, avoiding any Joule effect. It can be seen in Fig. 1 that no significant drift is observed during the time corresponding to most indentations (2 mn). The fluctuations, clearly visible in Fig. 1, could be reduced by isolating the apparatus from building vibrations. A complete description of the apparatus has been presented elsewhere.[4,5] The electrostatique applied force ranges between 10^{-7} N and 0·1 N, and the corresponding penetration depths between 0·3 nm, limited by the influence of building vibrations, and a few micrometers.

With this apparatus nanoindentation tests are fast and quite as convenient as conventional hardness ones, specimens of any shape being simply deposited on the upper plate of the apparatus (see Fig. 2) and pressed with a moderate mass. The first results are available a few minutes later and complex sequences can be easily programmed. Due to its thermal stability and reduced sensitivity to mechanical perturbations, the apparatus can be used in normal laboratory ambience. The shape of the diamond tip is calibrated, as usual, by indenting

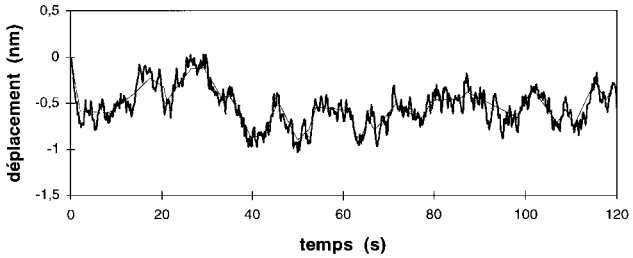

Fig. 1. Test of the thermal drift and the mechanical noise. Elapsed time: 120 s.

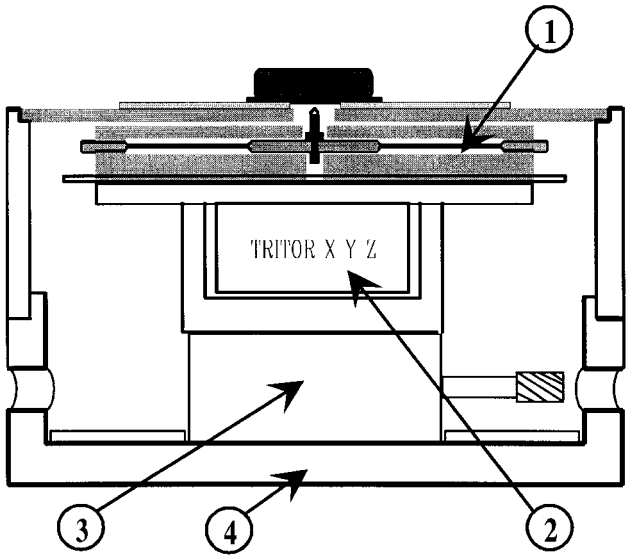

Fig. 2. A schematic drawing of the ND100 apparatus: 1. measurement head; 2. Piezo actuator (100×100×100 μm); 3. manual Z positioning; 4. frame.

well-polished fuzed silica samples and assuming a constant elastic modulus.

3 Hardness and elastic modulus determination

The nanoindentation hardness H, is taken as the mean pressure of the contact and corresponds to the Meyer's hardness:

$$H = \frac{F}{A} \tag{1}$$

F is the applied force and A the area of contact.

The contact area between the indenter tip and the sample can be derived from the penetration depth h_c, given that the shape function, $A(h_c)$ has been previously determined, for example by indenting a material of known Young's modulus.[6]

The penetration depth can be obtained from the experimental curves assuming that unloading is a purely elastic process.

In most materials the unloading curve can be fitted by a power law:

$$F = a(h - h_0)^m \tag{2}$$

with exponent m ranging between 1·2 and 1·7 and h_0 being the corrected plastic depth for the best fit.

The true penetration depth, h_c, is then given by:[7]

$$h_c = h_0 + \gamma(h_{max} - h_0) \tag{3}$$

with:

$$\gamma = \frac{1}{\sqrt{\pi}} \frac{\Gamma\left(\frac{n}{2} + \frac{1}{2}\right)}{\Gamma\left(\frac{n}{2} + 1\right)}$$

and:

$$n = \frac{1}{m - 1}$$

The fitting function given by eqn (2) is not linearly dependent of the unknowns and therefore a non linear least square method, like the Levenberg Marquadt's one,[8] has to be used. However, due to the particular form of the fitting function, the problem can be simplified and turned to be linear. Indeed, from the set of experimental points, it is possible to compute accurately at every point the primitive:

$$I(h) = \int F(h)\mathrm{d}h$$

Linearity is then obtained, with eqn (2), by dividing $I(h)$ by F:

$$\frac{I(h)}{F} = \frac{h - h_0}{m + 1}$$

and subsequently conventional linear least square methods can be used. The a constant is obtained from the values of F and h at the beginning of unloading:

$$a = \frac{F_{\max}}{(h_{\max} - h_0)^m}$$

and the stiffness is given by:

$$S = \frac{\mathrm{d}F}{\mathrm{d}h} = \frac{mF_{\max}}{(h_{\max} - h_0)}$$

avoiding to use a numerical derivation process.

The indentation elastic modulus E_r can then be obtained from the slope of the beginning of the unloading curve:[6]

$$E_r = \frac{\beta\sqrt{\pi}}{2\sqrt{\mathrm{A}}}\frac{\mathrm{d}F}{\mathrm{d}h} = \frac{\beta\sqrt{\pi}}{2\sqrt{\mathrm{A}}}\frac{mF_{\max}}{(h_{\max} - h_0)} \qquad (4)$$

β[9] is a geometrical coefficient equal to 1·034 for a triangular Berkovich indenter, $h_{\max}$ is the total penetration depth and E_r the indentation modulus, is a balance between the Young's modulus of the sample E_s and of the diamond indenter, E_i:

$$\frac{1}{E_r} = \frac{\left(1 - \nu_s^2\right)}{E_s} + \frac{\left(1 - \nu_i^2\right)}{E_i}$$

ν_s and ν_i are the respective Poisson's ratios.

With most apparatuses the experimental indentation curves must be corrected to take into account the compliance of the machine. With Doerner and Nix[10] it is possible to express the total compliance, C_t, as:

$$C_t = \frac{\mathrm{d}h}{\mathrm{d}F} = C_m + \frac{\beta\sqrt{\pi}}{2E_r\sqrt{A}} \qquad (5)$$

C_m being the frame compliance. A straight line is obtained when it is plotted versus the inverse square root of the surface of contact, given that the elastic modulus is constant. The intercept of this line with the compliance axes gives the value of the machine compliance. Common values are corresponding to a few nanometers per mN. When the value of C_m is determined the load–penetration curves can be corrected by replacing the measured penetration h by the quantity: $h - C_m F$.

The correction is very difficult when the Young's modulus is not constant, as for example in thin films, and it is much better to use an apparatus with a negligible frame compliance.

To derive, other mechanical properties as, σ_y yielding stress, σ_u ultimate stress (compressive stress at 30% plastic strain) or hardening ratio, from indentation curves it is necessary to treat the Berkovich indentation as a full 3D problem, as the finite element calculation by Larsson *et al.*[11] devoted to hard metals and ceramics. Their analysis supposes that the load versus penetration relationship is parabolic, which is generally not the case, as seen above, for very low applied loads.

Hardness is related to the yielding stress by the equation:

$$H = F/A = \alpha\sigma_y \qquad (6)$$

where σ_y is the compressive yield stress and α a constant about 3·3 in the absence of strain hardening and 2·08 for linear hardening. Thus the yield stress can be derived from the measure of the hardness or the mean contact pressure. More precisely the hardness for a Berkovich indentation[11] is given by:

$$H = 0{\cdot}245\sigma_y\left(1 + \frac{\sigma_u}{\sigma_y}\right)\left[1 + \ln\left(\frac{E\ \tan\ 24{\cdot}7^\circ}{3\sigma_y}\right)\right]$$

and the applied force:

$$F = \frac{1{\cdot}19}{\eta}\sigma_y\left(1 + \frac{\sigma_u}{\sigma_y}\right)(\tan\ 24{\cdot}7^\circ)^2 \times \left[1 + \ln\left(\frac{E\ \tan\ 24{\cdot}7^\circ}{3\sigma_y}\right)\right]h^2$$

η is a surface displacement factor obtained from a quadratic fitting the loading curve:

$$F = Ch^2 \qquad \eta = \frac{24{\cdot}5C}{H_v}$$

where H_v is the Vickers hardness given by:

$$H_v = \frac{0{\cdot}464F_{\max}}{d^2}$$

where $F_{\max}$ is the maximum applied load and d the diagonal length of a Vickers indentation. Thus, with this analysis, to derive the compressive yielding stress, it is necessary to determine first the Vickers' hardness, assumed to be a constant for a given material. Some values of this compressive yielding stress have been determined by Zeng *et al.*,[12] for ceramic materials and are listed below:

Fine-grained Al_2O_{30}	6·34 GPa
B_4C	12·00 GPa
TiB_2	9·84 GPa
W–6%Co	6·40 GPa
SiC	9·22 GPa
3%-Y-PSZ	5·28 GPa
10%-Y-PSZ	5·09 GPa
Hot-pressed Si_3N_4	7·01 GPa

From the unloading curve it is also possible to obtain an alternate expression for the Young's modulus:

$$E = \frac{(\mathrm{d}F/\mathrm{d}h)^2}{4f(\nu)F_{\max}} \qquad (7)$$

where $f(\nu)$ is a weak function of the Poisson's ratio equal to 2·196 for a Berkovich indentation and a Poisson's ratio of 0·25. The two values for the Young's modulus of fuzed silica, obtain from the above formula and from eqn (4), for the nanoindentation curves shown in Fig. 3, are, respectively, 55 and 72 Gpa. The difference between the result of eqn (7) and the litterature value (72 Gpa), is probably due to the fact that the exact shape of the indenter is not taken into account by (7) and that the exact value of the Poisson's ratio of silica is 0·17.

4 Experimental results

Different ceramic materials have been tested. Fused silica used as a calibration material, silicon, GaAs and MgO single crystals.

4.1 Fused silica

Figure 3 represents indentation curves obtained in a opticaly polished fused silica sample. It can be seen that the deformation is quasi elastic for applied forces up to 2 mN, corresponding to total penetrations of about 90 nm. For a higher applied force (7 mN) the plastic deformation appears clearly. The Young's modulus, assuming a Poisson's ratio of 0·17 and the nanoindentation hardness are plotted versus the penetration depth in Figs 4 and 5. The Young's modulus is constant, which is not surprising since it has been used to calibrate the shape of the tip, while the hardness is observed to decrease when the penetration depth goes to zero.

This can be predicted from Hertz[13] theory of contact between elastic bodies, which is the case, as seen above, of fused silica under very low applied forces.

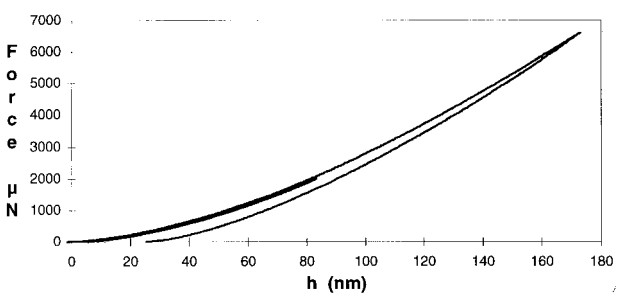

Fig. 3. Successive indentation curves in a fuzed silica specimen, with 80 and 175 penetration depths.

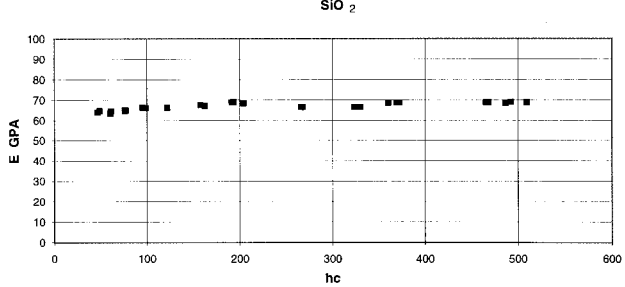

Fig. 4. Young's modulus of fuzed silica measured as a function of the penetration depth.

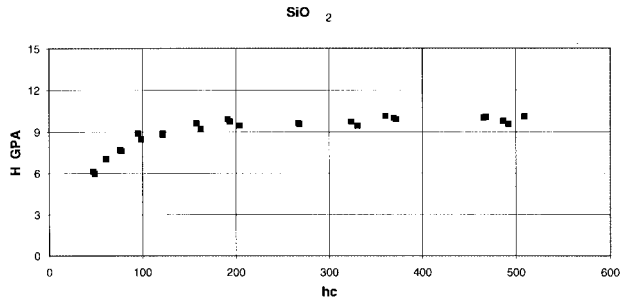

Fig. 5. Hardness of fuzed silica measured as a function of the penetration depth, showing the decrease at low penetration depths.

For a blunt indenter with a shape function:

$$z = c\rho^{\mathrm{n}}$$

the Hertzian hardness is:

$$H = \frac{2E_{\mathrm{r}}}{\sqrt{\pi}} c^{-\frac{1}{n}} \frac{n}{n+1} \frac{\Gamma(n/2+1)}{\Gamma(n/2+1/2)} h_{\mathrm{c}}^{1-1/n}$$

It appears that the Hertzian hardness is constant, as a function of the penetration depth, only for conical or pyramidal indenters, corresponding to $n = 1$, whereas for non geometrically similar indenters, $n > 1$, the hardness vanishes when the penetration depth h_{c} falls to zero; that is the case of real indenters which can be approximated by spheres ($n = 2$) for very small penetration depths.

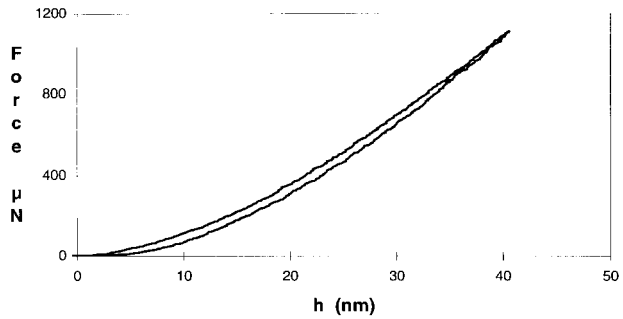

Fig. 6. Low depth indentation in a (100) silicon single crystal, exhibiting an almost elastic behavior.

4.2 Silicon

Under low applied loads silicon crystals behave almost elastically as shown in Fig. 6. Plasticity becomes significant at loads lower than for fused silica as can be seen comparing Figs 3 and 6. This is somewhat surprising since the tested (100) wafers were almost dislocation free and since silicon is known to be harder than silica. At higher stresses, as shown in Fig. 7, a sharp kick-back or pop-out appears in the unloading curves as previously reported.[14]

Because of the very low roughness of the tested surfaces, lower than 2 nm as checked by atomic force microscopy, and due to the fact that no trace of dislocation motion have been detected (no slip lines) around the indents, the plasticity is thought to arise from a densification process rather than from dislocation activity.[15] Similarly the pop-out during unloading would be associated to a related undensification process, during loading the Si1 cubic diamond structure transforms into a 27% denser Si2 tin-like structure, whereas at the pop-out that new phase returns to a less dense state corresponding to the new cubic Si3 phase only 8% denser that the initial diamond structure. An alternative explanation had been proposed for the pop-out phenomenon: the closure of microcracks nucleated during loading, but that hypothesis has certainly to be rejected since no cracks could be detected around the indents.

The Young's modulus and the hardness of the tested (100) wafers are plotted in Figs 8 and 9. The previously mentioned decrease in hardness at very low depth, corresponding to a mostly elastic behavior, is observed again. The values of both the elastic modulus (135 Gpa) and the hardness (12·5 Gpa) are in good agreement with earlier results.[15] The last value is compatible with the hydrostatic pressures for the two phase transforms, obtained from high pressure experiments[16] ranging between 8 and 12·5 GPa. Thus it seems confirmed that, in the case of silicon, the critical resolved shear stress for dislocation nucleation exceeds the hydrostatic pressure for densification. The reverse transforms associated to the pop-out during unloading has been found time dependent as shown in Fig. 10. The fastest test (curve a), running at a velocity of 1·6 nm s^{-1} and corresponding to the highest applied force (24 mN), shows no clear pop-out, only a slow inflexion in the unloading part of the curve, whereas the slowest one (0.6 nm s^{-1}), corresponding to a lower applied force (20 mN) exhibits a marked pop-out. That tendency is systematic and seems to indicate that the transforms are thermally activated.

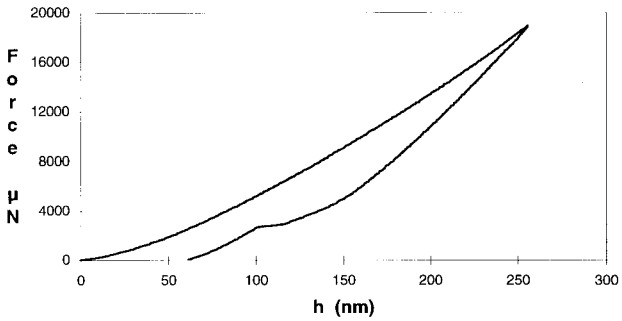

Fig. 7. Higher depth indentation curve in the silicon single crystal showing the pop-out in the unloading portion of the curve.

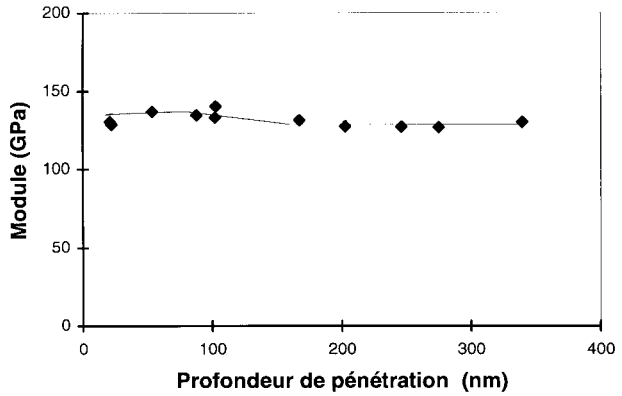

Fig. 8. Young's modulus of the silicon single crystal, plotted as a function of the penetration depth.

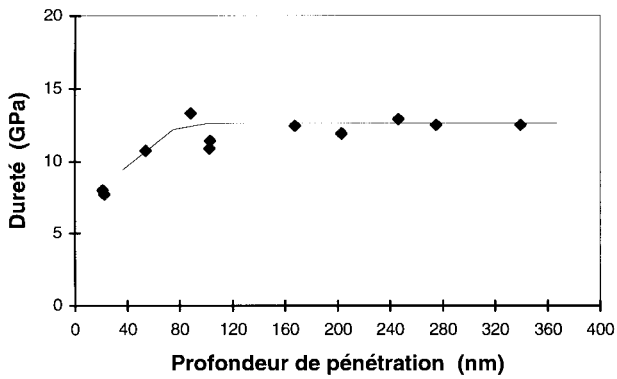

Fig. 9. Hardness of the silicon single crystal, plotted as a function of the penetration depth.

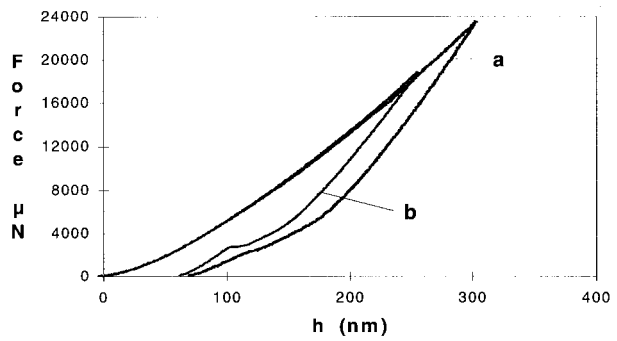

Fig. 10. Indentation curves, at different velocities, in the silicon single crystal. The pop-out tends to disappear when the velocity is increased.

When performing successive full loading–unloading sequences (see Figs 11 and 12) the pop-out is observed to gradually disapear, resulting in an almost elastic behavior, indicating that the Si2 phase gradually transforms into the less dense Si3 phase. During successive cycles Hainsworth *et al.*[15] observed a gradual increase in the maximum penetration depth. In agreement with earlier work,[14] we did not observe that effect which may be due to uncontrolled thermal drifts. From this observation one may question the validity of the procedures proposed to eliminate the influence of thermal drifts, since they have chance to be unpredicable. The insensivity of our apparatus to thermal drifts is illustrated by the fact that, despite the tip is completly removed from the sample and positioned at about 200 nm from the surface between two consecutive cycles, successive loading parts of the curves are perfectly superimposed onto the preceeding unloading parts.

4.3 GaAs

Higly polished as-received (100) GaAs wafers have been tested. As seen in Fig. 13, no kick-back or pop-out was detected in GaAs specimens but, as previously observed[17] a large pop-in was observed during loading. This pop-in appears highly reproducible in a given specimen. It is remarkable that the pop-in is much larger (up to 30 nm) and appears at much higher stresses than previously observed.[17] This may be due either to the shape of the extremity of the indenter or to the fact that the roughness of the wafer was very low and almost defect free. The yield point probably corresponds to dislocation nucleation in a free defect volume beneath the indenter.

The measured Young's modulus (120 Gpa) is in a good agreement with tabulated values.[18] The hardness is plotted in Fig. 14 as a function of the penetration depth, and it can be seen that it reaches a very high value (12 Gpa) before the yield point and then drops to a constant much lower value (8 Gpa). As seen before the decrease for the low penetration depths is due to the elastic behavior of the material. If we assume, for low penetration depths, a spherical indenter, the maximum shear stress beneath the indenter is 0·47 H,[13] close to the theoretical strength of the material.

Thus in GaAs no densification process could be observed despite the high values of the hardness measured before the yield point.

A ceramic material with a much higher elastic modulus, MgO, was then examined.

4.4 MgO

Presumably defect free {100} cleaved surfaces of a MgO single crystal were indented and then observed by atomic force microscopy to detect the traces of dislocation activity around the indents. The tests and the subsequent observations had to be done immediately after the surfaces were

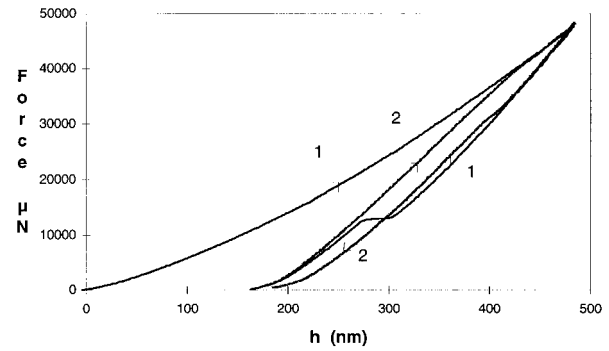

Fig. 11. Successive loading–unloading sequences on the silicon single crystal, showing the progressive disappearance of the pop-out.

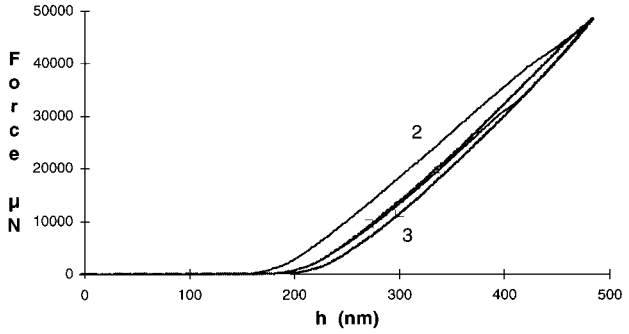

Fig. 12. Successive loading–unloading sequences on the silicon single crystal, showing the progressive disappearance of the pop-out.

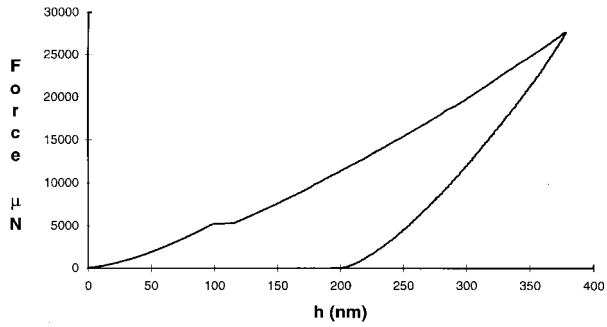

Fig. 13. Indentation curve in a (100) GaAs single crystal showing a large pop-in during loading.

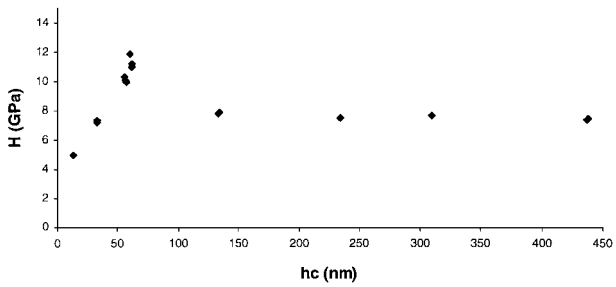

Fig. 14. Hardness of the GaAs single crystal, showing a sharp decrease corresponding to the pop-in.

cleaved since the initially clean surfaces were very fastly contaminated.

The cleaved planes presented a lot of steps, because of the presence of preexisting dislocations, limiting flat surfaces suitable for indentation and subsequent examinations. Indentation arrays ($100 \times 100\,\mu$m), limited by large indents (80 mN) easily detected with an optical microscope, were performed with different penetration depths. A large distance was maintained between consecutive indents (20 μm) to avoid any interaction, as confirmed by the presence of large pop-ins (Fig. 15) for all the tests corresponding to sufficiently high applied loads. At lower loads (Fig. 16) the deformation is again almost completely elastic. The Young's modulus was found equal to 310 Gpa and very high hardness values were measured before the yield point (30 Gpa), close to the theoretical strength, as in GaAs. After the yield point the hardness falls down to 13 Gpa and then remains sensibly constant. The decrease of the hardness, due to the elastic behavior, for the lower penetrations is observed again. In MgO the extent of the pop-in, measured in the force controlled mode (Fig. 15), is very large, up to 35 nm, corresponding, for a $<100>$ Burgers vector, to the nucleation of about 90 dislocation loops, for a lattice parameter of 0·421 nm.

As seen in Fig. 17, dislocation rosettes with four arms parallel to $<100>$ directions, like those observed around Vickers indents[19] despite the three-fold symmetry of the Berkovich indenter, are formed at the surface. The preceeding image corresponds to a penetration depth of 315 nm, for a maximum applied force of 80 mN. The four arms of the rosette are clearly visible and made of dislocation steps also parallel to $<100>$ directions. Three profiles have been measured, by atomic force microscopy, on one of the arms. It has been shown that the U-shaped arms, with flat bottom, gently sloping up to the surface. The fine structure of the arms corresponds to $<100>$ slip lines mostly concentrated at the edge of the arms the central part being completely flat. In Fig. 19, in a smaller indent, corresponding to an applied force of 8 mN, it can be seen that the rosette arms extend inside the indent, showing that two opposite arms develop simultaneously, since the slip lines propagate from one arm to the opposite one crossing over the indent.

Other slip lines, in $<100>$ directions are equally visible. They have previously been observed by Armstrong[19] around Vickers indents. As

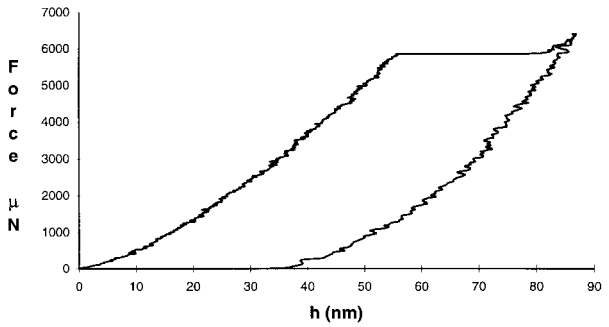

Fig. 15. Indentation curve in a (100) cleaved surface of a MgO single crystal with a large pop-in during loading.

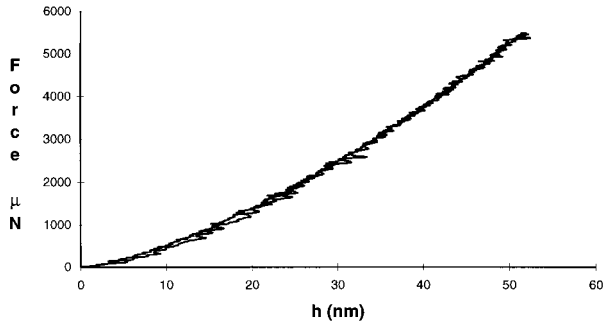

Fig. 16. Elastic behavior of MgO for low penetration depth.

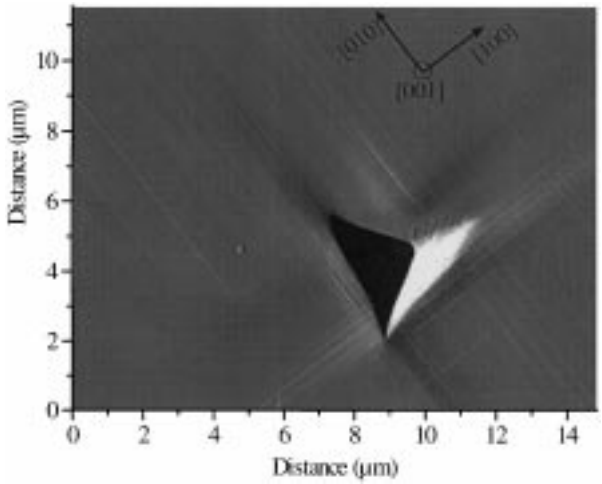

Fig. 17. Atomic force microscope image (tapping mode) of a large indent in the MgO single crystal. The four rosette arms are clearly visible.

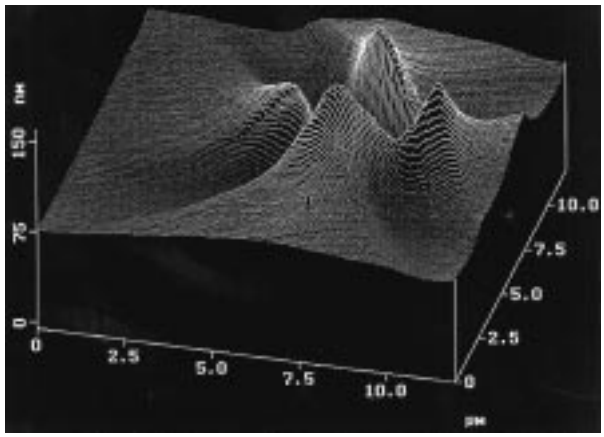

Fig. 18. Another view of the preceeding indent showing the pilling-up between the rosette arms.

previously mentionned the rosette arms have a flat bottom exempt of steps and the four bottoms intersect in a non deformed depressed square at the centre of the indent. Finally the material is pilled-up at the four corners limited by the rosette arms, as seen in Fig. 18, indicating that the matter around indentations in hard materials is submitted to both pilling-up between the rosette arms and to sinking down inside the arms.

A two stages mechanism is proposed to explain these observations. The first stage is a punching mechanism: in the volume under the indenter, free of dislocations, no Frank–Read sources can be activated. Interstitial loops, with $[00\bar{1}]$ Burgers vectors, are suddenly created when the stress approaches the theorical strength and the indenter penetrates rapidly in the material, which correspond to the pop-in observed in the loading part of the nanoindentation curves. These loops are pilled-up beneath the indenter. However $[00\bar{1}]$ Burgers vectors are not stable in MgO and the loops tend to adopt a square form to dissociate in two dislocations, with $<110>$ Burgers vectors, lying in $\{110\}$ planes:

$$[00\bar{1}] = \frac{1}{2}[01\bar{1}] + \frac{1}{2}[0\bar{1}\bar{1}]$$

The new dislocations are then glissile in their $\{110\}$ planes, belonging to the primary glide system in MgO. The dislocations being pinned at the corners of the square they behave as Frank–Read sources and propagate in $\{110\}$ planes making an angle of 45° relative to the surface. When they reach the surface, the steps observed along $<100>$ directions

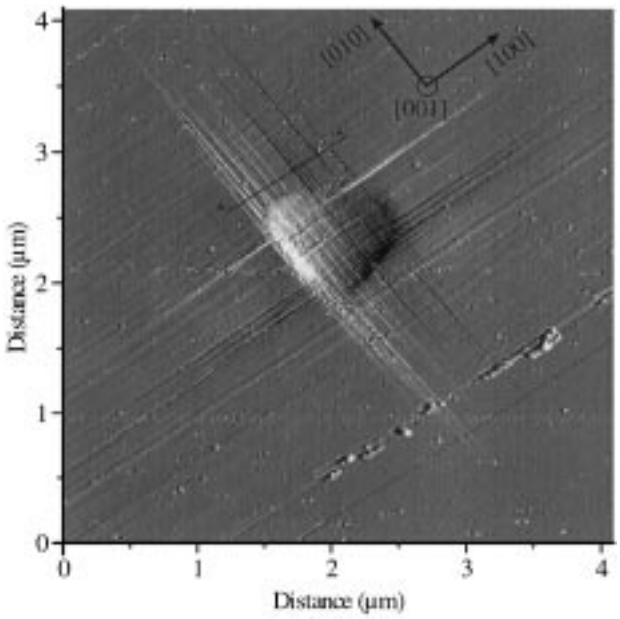

Fig. 19. Small indent in the MgO single crystal, showing the slip lines crossing over the indent.

are formed. An enlarge image of the initial square loop is thus formed at the surface.

The second step corresponds to the formation of the rosettes. When the deformation goes on, the surface about the initial indentation created during the pop-in is submitted to important shear stresses that cannot be accomodated by the few interstitial loops previously created, despite the fact they are still active Frank–Read sources. Under the shear stress U-shaped loops are created at the surface, whose upward arms are screw segments, which extend in opposite $\langle 100 \rangle$ directions, the steps parallel to the rosette arms are thus formed. Further details of the mechanism will be presented elsewhere.

5 Conclusion

Nanoindentation testing is a powerful technique for the study of mechanical properties of small volumes of materials. For brittle high strength ones, like ceramics, it is one of the few available methods to determine quantities as yield stress, ultimate stress or strain hardening ratio. The next step, since fiable apparatus are now available, will certainly be further developments of full 3D analysis for Berkovich indentations, taking into account the exact shape of the indenter and the anisotropy of the materials. One of the main drawback for very low penetration depths tests is however, the fact they require very low roughness and contamination free surfaces. Several mechanisms have been proposed to take into account the special features of the studied materials. For silicon the plasticity is probably due to a stress induced densification process whereas, in GaAs and MgO crystal, it is associated to the abrupt creation of intersitial dislocation loops, beneath the indenter, at stresses close to the theoretical strength.

References

1. Pethica, J., Hutchings, R. and Oliver, W. C., Hardness measurement at penetration depths as small as 20 nm. *Phil. Mag*., 1983, **A48**(4), 583–606.
2. Bushan, B., Kulkarni, A., Bonin, W. and Wyrobek, J., Nanoindentation and picoindentation measurements using a capacitive transducer in atomic force microscopy. *Phil. Mag*, 1996, **A74**, 1117–1128.
3. Yanagisawa, M. and Motomura, Y., An ultramicro indentation hardness tester and its application to thin films. *Lubrification Eng*., 1987, **1**, 52–56.
4. Woirgard, J. and Dargenton, J. C., A new proposal for design of high accuracy nano-indenters. *Meas. Sci. Technol*., 1995, **6**, 16–21.
5. Dargenton, J. C. and Woirgard, J., Description d'un nanoindenteur á force electrostatique. *Journ. Phys III*, 1996, **6**, 1247–1260.
6. Oliver, W. C. and Pharr, G. M., An improved technique for determining hardness and elastic modulus using load

and displacement sensing indentation experiments. *J. Mater. Res.*, 1992, **7**, 1564–1583.
7. Dargenton, J. C., Réalisation et mise au point d'un nanoindenteur de conception nouvelle. Ph.D. Thesis, Université de Poiters, France, 1996.
8. Press, W. H., Flannery, B. P., Teukolsk, S. A. and Vetterling, W. T., *Numerical Receipes in C*. Cambridge University PressCambridge, 1988
9. King, R. B., Elastic analysis of some punch problems for a layered medium. *Int. Journ. Solids. Struct.*, 1987, **23**, 1657–1664.
10. Doerner, M. F. and Nix, W. D., A method for interpretating the data from depth sensing indentation instruments. *J. Mater. Res.*, 1986, **1**, 601–609.
11. Larsson, P. L., Giannakopoulos, A., Soderlund, E., Rowcliffe, D. J. and Vestergaardt, R., Analysis of Berkovich indentation. *Journ. Solids Struct.*, 1996, **33**, 221–248.
12. Zeng, K., Doderlund, E, Giannakopoulos, A. E. and Rowcliffe, D. J., Controlled indentation: a general approach to determine mechanical properties of brittle materials. *Acta. Metall. Mater*, 1996, **44**, 1127–1141.
13. Johnson, K. L., *Contact Mechanics*. Cambridge University Press, Cambridge, 1985.
14. Pharr, G. M., Oliver, W. C. and Clarke, D. R., Hysteresis discontinuty in the indentation load-displacement behavior of silicon. *Scripta Metall.*, 1989, **23**, 1949–1952.
15. Hainsworth, S., Whitehead, A. J. and Page, T. F., The nanoindentation response of silicon and related structurally similar materials. In R. C. Bradt, C. A. Brookes and J. L. Routbart (eds), *Plastic Deformation in Ceramics*. Plenum Press, London, 1994. p. 173.
16. Gridneva, I. V., Milman, Y. and Trefilov, V. I., Phase transition in diamond structure crystals during hardness measurements. *Phys. Stat. Sol (a)*, 1972, **14**, 177–182.
17. Mann, A. B. and Pethica, J. B., Dislocation nucleation and multiplication during nanoindentation testing. *Mat. Res. Symp.*, 1997, **436**, 153–158.
18. Simmons, G. and Wang, H., *Single Crystal Elastic Constants and Calculated Aggregates Properties: A Handbook*. M. I. T. Press, Cambridge, MA, 1976.
19. Armstrong, R. W. and Wu, C., Lattice misorientation and displaced volumes for microharness indentation in MgO crystals. *Journal of Amer. Ceram. Soc.*, 1978, **61**, 102–106.